Journal of Sol-Gel Science and Technology
https://doi.org/10.1007/s10971-018-4763-2

ORIGINAL PAPER: SOL-GEL AND HYBRID MATERIALS FOR BIOLOGICAL AND HEALTH (MEDICAL) APPLICATIONS

Uptake of curcumin by supported metal oxides (CaO and MgO) mesoporous silica materials

Issa M. El-Nahhal[1] · Jamil K. Salem[1] · Nihal S. Tabasi[1]

Received: 3 April 2018 / Accepted: 24 July 2018

Abstract

Supported metal oxides (CaO and MgO) mesoporous silica were synthesized using impregnation method. Curcumin uptake capacity by metal oxides (CaO and MgO) supported mesoporous silica were determined using batch method. The structural properties of these materials were investigated using several characterization techniques such as FTIR, XRD, SAXS, TEM, TGA, and UV-vis. UV-vis analysis shows that curcumin have higher uptake capacity for CaO than MgO/mesoporous silica. It also found that the hexagonal-SiO_2-SBA-15 have the highest capacity for curcumin than other lamellar-SiO_2 structures.

Graphical Abstract

Supported metal oxides of two types mesoporous silica structures(hexagonal and lamellar) are prepared by impregnation method. Metal(II) curcumin complexes are formed upon treatment of curcumin with supported metal oxides mesoporous silica.

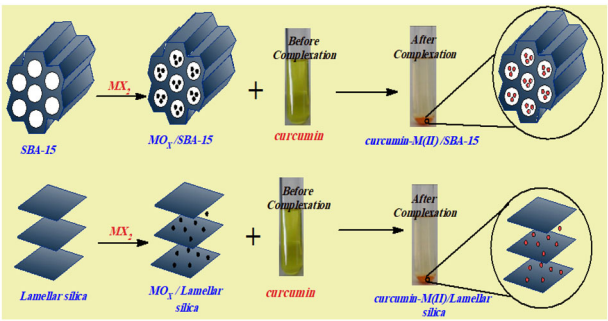

Highlights

- Metal oxides (CaO and MgO) supported mesoporous silica were synthesized via impregnation method.
- Curcumin uptake capacity is depended on the nature of metal oxide and the type of mesoporous silica.
- Free curcumin was released from mesoporous silica by treatment of immobilized Ca(II) & Mg(II) curcumin complexes with HCl.
- SAXS and TEM results showed that metal oxides are introduced into the mesoporous silica network.
- XRD showed that all metal oxides were in crystalline form faced center cubic CaO and MgO.

Keywords Curcumin · Mesoporous silica · Uptake of curcumin · Curcumin metal complexes · CaO and MgO/mesoporous silica

✉ Issa M. El-Nahhal
issanahhal@hotmail.com

[1] Department of Chemistry, Al-Azhar University, P.O. Box 1277 Gaza, Palestine

Published online: 06 August 2018

1 Introduction

Curcumin is the major curcuminoid and the main bioactive component of Curcuma longa. Curcumin has received ample attention as potential drug because of various pharmaceutical applications as anti-oxidant [1], anti-inflammatory [2], anti-carcinogenic agent [3], anti-Alzheimer's disease [4], anti-cystic fibrosis [5], anti-neoplastic, and wound-healing effects [6] and anti-angiogenic activities [7]. Major problem with curcumin is its low bioavailability for the treatment of these chronic diseases. Curcumin is very poorly soluble in water which reducing its effectiveness as a drug [8]. For that reason, various methods are being developed to enhance curcumin solubility, bioavailability and effectiveness of the drug during its delivery [9, 10]. Different approaches for developing novel drug-delivery systems is the use of mesoporous silica materials because of their interesting properties, such as: variable and controllable particle sizes that lead to an easy endocytosis by cells and possess low cytotoxicity, stability to heat, pH, mechanical stress and chemical degradations, tunable narrow pore size distribution and pore diameter that lead to a rational loading of different drug molecules, high surface area which allows of drug incorporation. For all these reasons, silica-based mesoporous materials have been used for curcumin delivery where it demonstrates that all the curcumin loaded materials, show the inhibition of cancer cell viability and migration compared to free curcumin, suggesting the efficacy of the drug delivery system vehicles in various biomedical applications[11]. It has reported that mesoporous phosphosilicate nanoparticles of hollow sphere architecture have been prepared hydrothermally for the first time under acidic pH conditions and this material is found to be efficient in encapsulating an antibiotic drug and its controlled release at physiological pH for possible cargo delivery applications[12].

Different mesoporous silica based formulations have been recently developed to enhance bioavailability of curcumin as drug [13, 14]. Mesoporous silica with high surface area, large pore volume and narrow pore size distribution [15] are highly promise for drug delivery systems [16]. Chemical modification of silica pore channels with metal and metal oxides led to new materials with unique physical, chemical and catalytic properties [17]. Incorporation of metal oxide in mesoporous silica has been a promising field of research such as catalysis [18], optics [19] and drug delivery [20]. Two main methods are developed to introduce metal oxides into the silica mesopores. Post modification method, which involves a wet impregnation of metal precursor into the existing mesoporous silica followed by its reduction to metal or metal oxides nanoparticles [21–23], and direct modification method, which involves a direct addition of metal precursor into the precursor solution of mesoporous silica [24, 25]. In our present research we aimed to fabricate an inert mesoporous system with avoiding hazard materials with also ease for loading and unloading curcumin when needed. Four different mesoporous silica materials were firstly prepared using different triblock copolymer surfactants (Pluronic P123 form hexagonal structures whereas L81, L61, and L31 form lamellar structures)[26]. Then, supported metal oxides (CaO and MgO)/mesoporous silica were synthesized using impregnation method. As calcium and magnesium are main constituents of human body, hence we exploited the reversible calcium and magnesium chelate formation tendency of divalent calcium and magnesium to load and unload curcumin molecules. In this research, uptake percentage of curcumin, by two different metal oxides supported onto four different mesoporous silica (hexagonal and lamellar structures) are investigated. It is found that curcumin uptake % is depend on the metal oxide and the type of mesoporous silica. The systematic procedure for impregnation synthesis of metal oxides and curcumin uptake is presented in Scheme 1. The synthesized supported metal oxides-mesoporous silica materials and their curcumin complexes were characterized using several methods and

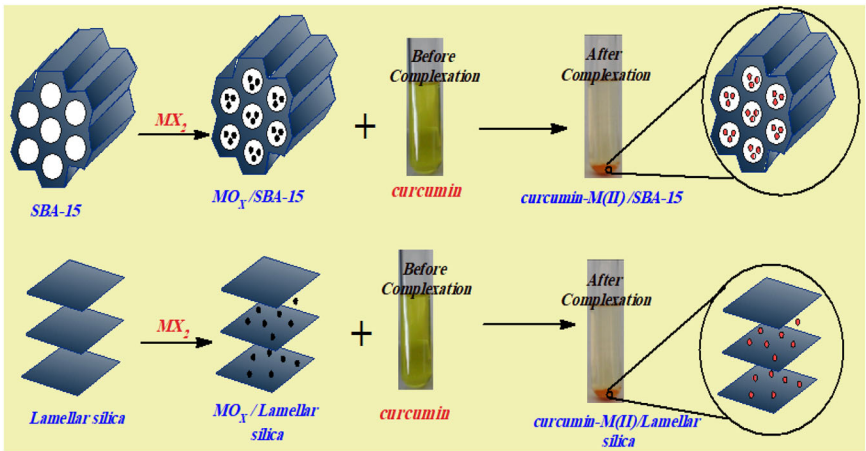

Scheme 1 Description of synthesis of supported metal oxide-mesoporous silica via impregnation method and curcumin uptake

techniques to examine their structural properties. These methods include Fourier transform infrared spectroscopy (FTIR), X-ray diffraction (XRD), small angle X-ray scattering (SAXS), transmission electron microscopy (TEM), thermal gravimetric analysis (TGA) and ultraviolet-visible spectroscopy (UV–vis).

2 Experimental

2.1 Materials

All the chemicals used were analytical grade and directly used as received without further purification. Triblock copolymer Pluronic P123 (EO_{20} PO_{70} EO_{20}, 99%), Pluronic L81 (EO_3 PO_{43} EO_3, 99%), Pluronic L61 (EO_2 PO_{31} EO_2, 99%), Pluronic L31 (EO_2 PO_{16} EO_2, 99%), Tetraethoxysilane (TEOS) ($Si(OC_2H_5)_4$), absolute ethanol (C_2H_6O) were purchased from Aldrich company. Magnesium acetate tetra-hydrate ($Mg(CH_3COO)_2.4H_2O$)), curcumin ($C_{21}H_{20}O_6$) were purchased from Sigma-Aldrich Company. Calcium carbonate ($CaCO_3$) was purchased from Sigma Company. Hydrochloric acid (HCl, 37%) and acetic acid (CH_3COOH, 99.8%) were purchased from Merck Company. All the glassware used in this experimental work washed with distilled water and dried at 100 °C.

2.2 Methodology

Infrared spectra for the materials were recorded on a Perkin-Elmer FTIR spectrometer using KBr disk in the range 4000–400 cm^{-1}. TGA was carried out using Mettler Toledo TGA/SDTA 851e analyzer in the range of 25–600 °C of heat rate of 10 °C/min. The system was purged with nitrogen using a flow rate of 50 mL/min. Powder XRD patterns were recorded on Analytical Expert Pro diffractometer utilizing Cu Kα radiation ($k = 1.54$ Å). The TEM analysis was performed with JEM2010 (JEOL) transmission electron microscope with energy-dispersive X-ray spectrometer INCA (Oxford Instruments). Ultraviolet–visible absorption spectra were recorded on a UV–vis spectrophotometer Shimadzu, UV-2400 in the wavelength range from 200 to 800 nm.

2.3 Synthesis

2.3.1 Synthesis of mesoporous silica

Mesoporous silica (hexagonal and lamellar structures) were synthesized as previously reported in literature [26], 4.0 g of nonionic triblock copolymer Pluronic surfactant (P123, L81, L61, and L31) was dispersed in 40 mL of deionized water at 10 °C for 1 h. Then (60 mL) of 2 M HCl was added slowly to the surfactant solution under the same conditions. 8.8 mL (39.4 mmol) of TEOS was added to the stirred solution under the same conditions. The mixture was stirred for 24 hat room temperature. The mixture was autoclaved at 100 °C for 48 h. The materials were calcinated at 500 °C for 3 h. The synthesized materials are labeled as SBA-15, SiO_2-L81, SiO_2-L61, and SiO_2-L31, respectively.

2.3.2 Synthesis of supported metal oxides/mesoporous silica

The supported metal oxides (CaO and MgO)/mesoporous silica materials were prepared using impregnation method [22, 23]. (30% wt./wt.) of the appropriate metal acetate was dissolved in deionized water. Subsequently, 0.70 g of calcinated mesoporous silica was added to the previous solutions. The mixture was stirred for 2 h at room temperature, and then was stirred at 80 °C to dryness. The final product was dried at 100 °C overnight. The materials were calcinated at 600 °C for 4 h. The obtained materials were labeled as CaO/SBA-15, CaO/SiO_2-L81, CaO/SiO_2-L61, CaO/SiO_2-L31, MgO/SBA-15, MgO/SiO_2-L81, MgO/SiO_2-L61 and MgO/SiO_2-L31.

2.3.3 Determination of curcumin uptake

Curcumin is present in three structures ketone, enol and anion forms (Scheme 2). Curcumin uptake for CaO and MgO/mesoporous silica was determined using batch method. 0.2 g of supported metal oxide/mesoporous silica was shaking with 25 mL of ($6*10^{-5}$ M) ethanolic curcumin solution for 72 h. Then, curcumin-metal(II) complexes/mesoporous silica were separated by centrifuge (3500 rpm for 15 min), were washed with 5 mL ethanol and were dried at 80 °C. The curcumin uptake capacity was quantified measured by spectrophotometric method, the results are

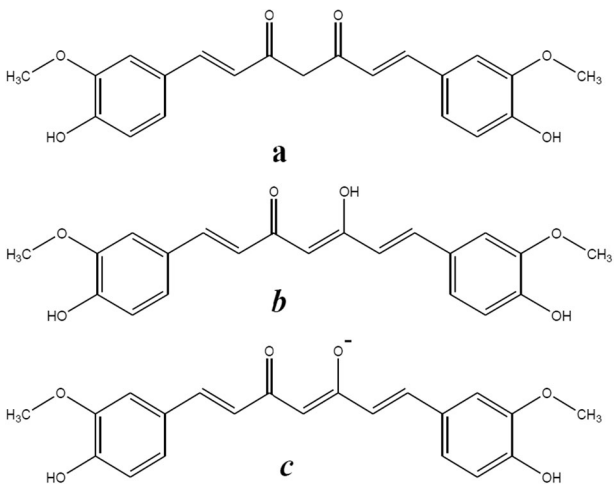

Scheme 2 Structure of curcumin in the **a** ketone **b** enol, and **c** anion forms

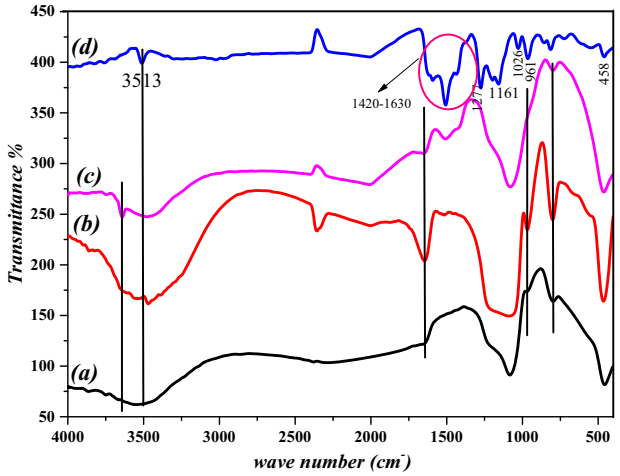

Fig. 1 FTIR spectra of **a** SiO_2-L81, **b** CaO/SiO_2-L81, **c** curcumin-Ca (II)/SiO_2-L81, and **d** curcumin

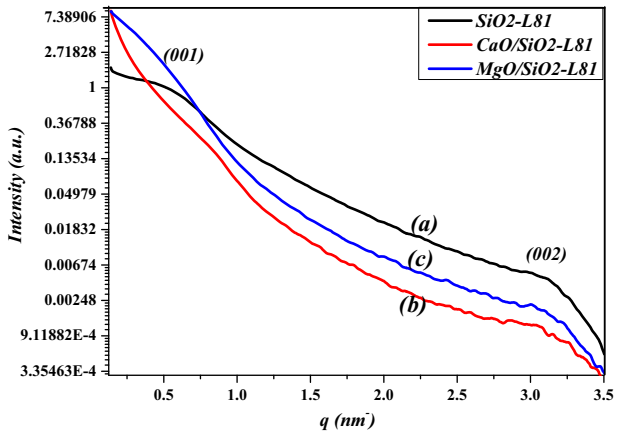

Fig. 4 SAXS pattern of **a** SiO_2-L81, **b** CaO/SiO_2-L81, and **c** MgO/SiO_2-L81

given in Fig. 12. A complete release of curcumin was also observed upon mild acidic treatment the loaded samples, where the orange color of the Ca(II) curcumin complex is converted into yellow color of free curcumin.

3 Result and discussion

3.1 Synthesis

Supported metal oxides (CaO and MgO)/mesoporous silica were prepared using post synthesis (impregnation) method [22, 23]. In this method, mesoporous silica materials (hexagonal and lamellar structures) were firstly prepared using copolymer surfactants (Pluronic P123, L81, L61, and L31) as previously reported [26]. Metal precursor (CaX_2 and MgX_2) was loaded into/onto silica and then metal precursor was decomposed by thermal treatment as shown in Scheme

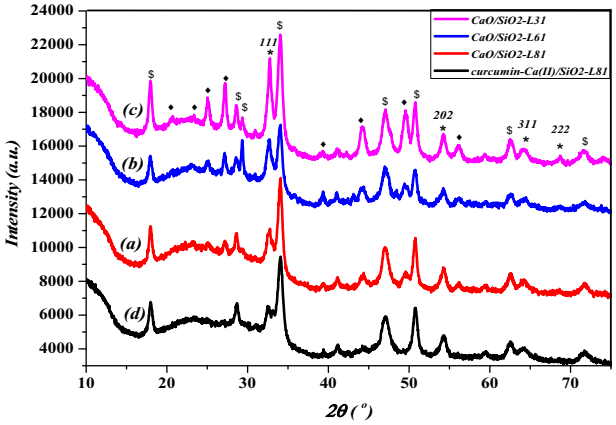

Fig. 2 XRD pattern of **a** CaO/SiO_2-L81, **b** CaO/SiO_2-L61, **c** CaO/SiO_2-L31, and **d** curcumin-Ca(II)/SiO_2-L81

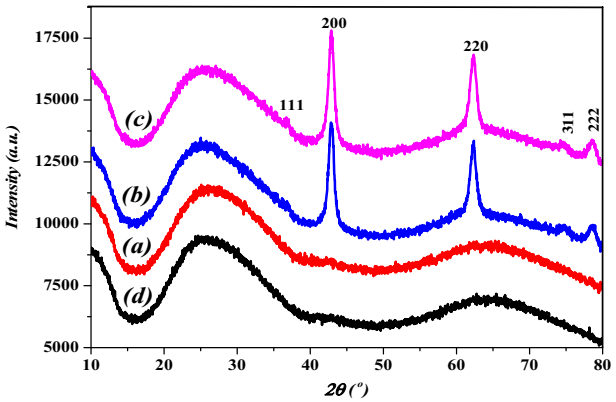

Fig. 3 XRD pattern of **a** MgO/SiO_2-L81, **b** MgO/SiO_2-L61, **c** MgO/SiO_2-L31, and **d** curcumin-Mg(II)/SiO_2-L81

1. Curcumin molecules were loaded into mesoporous silica by treatment of supported metal oxide/mesoporous silica with curcumin ethanolic solution under shaking to accelerate the reaction. Curcumin Ca(II) and Mg(II) complexes were formed. In a contrast to this present research, curcumin was previously introduced into amine APTES coated super paramagnetic iron oxide (magnetite) nanoparticles [27].

3.2 Fourier transform infrared (FTIR)

FTIR spectra of SiO_2-L81, CaO/SiO_2-L81, curcumin-Ca (II)/SiO_2-L81 and free curcumin materials are given in Fig. 1a-d. The spectrum of CaO/SiO_2-L81 shows an absorption at 3643 and 3506 cm^{-1} of $Ca(OH)_2$ and ν(O–H) vibration of hydrogen-bonded between adsorbed water and silica surfaces. A broad band in range of 3400–3600 cm^{-1} in Fig. 1a is due to ν(O–H) vibration of hydrogen-bonded between adsorbed water and MO and silica surfaces. The weak peak at 1645 cm^{-1} (Fig. 1a-c) is probably due to δ(O–H) vibration [28, 29]. In Fig. 1a-c, the three peaks at 1085 (broad), 800, and 459 cm^{-1} are due to asymmetric stretching,

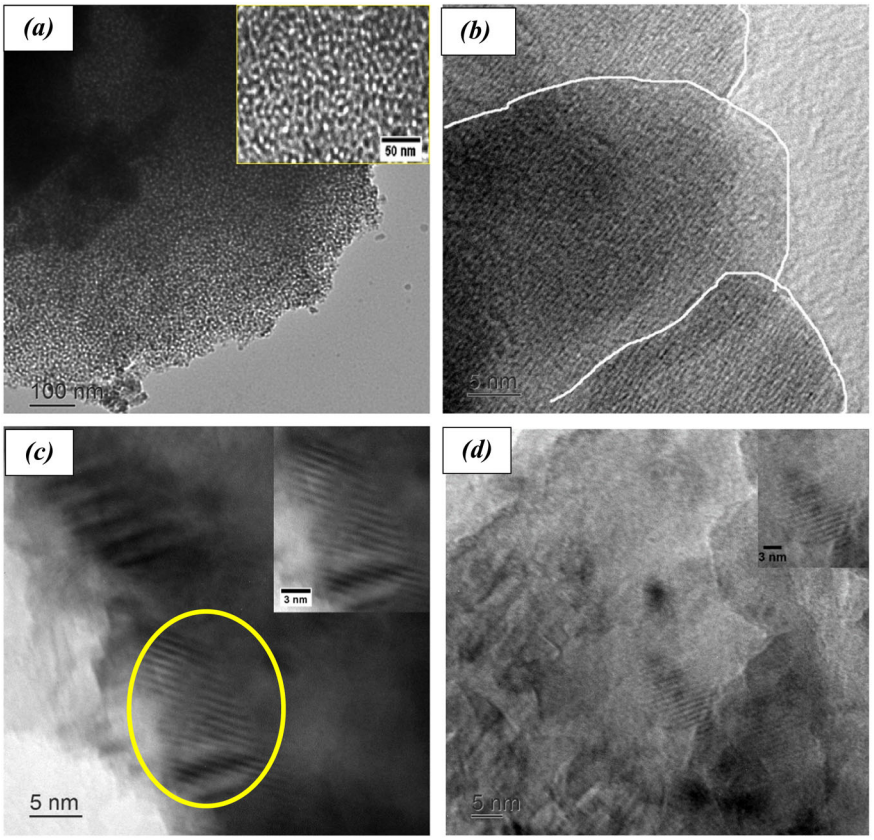

Fig. 5 TEM image of **a** (low-resolution) SiO_2-L81, **b** (high-resolution) SiO_2-L81, **c** CaO/SiO_2-L81, and **d** MgO/SiO_2-L81

symmetric stretching and bending of Si–O–Si vibrations from silica network, respectively [28, 29]. An absorption peak at 960 cm^{-1} is assigned due to ν(Si–OH) of free silanol groups. The decrease of peak intensities of absorption peaks at 3400–3600 cm^{-1}, at 1645 cm^{-1} and 960 cm^{-1} (Fig. 1c) is probably associated complexation of curcumin with calcium ions into/onto the silica pores.MO/SiO_2-L81. In Fig. 1d, several peaks around 1511 and 1428 cm^{-1} are associated with presence of the curcumin [28]. The presence of a shoulder at about 560 cm^{-1}in Fig. 1b is related to (Ca–O) vibration [30]. The absence of this shoulder at 510 cm^{-1} (Fig. 1c) is a good evidence for the formation of curcumin-calcium(II) complex. Other curcumin peaks are probably obscured within broad, intense mesoporous silica absorption peaks [31]. There is no presence of absorption peaks related to surfactant, which gives a good evidence that pluronic surfactants are totally removed upon calcination.

FTIR spectra of curcumin (Fig. 1d) shows the presence of a sharp absorption peak at 3513 cm^{-1} related to phenolic (–OH) stretching vibration [31]. The small peaks at 3023 and 2970 cm^{-1} are due to the aromatic (C–H) and methyl (C–H) stretching vibration, respectively [31]. The most prominent band in the IR spectrum at 1420-1630 cm^{-1} attributed to the mixture of stretching vibrations of (C=C) and C=O stretching vibration of curcumin [31–33]. C=O stretching vibration appears at low frequency due to high conjugation system. The peaks at 1277 cm^{-1} is attributed to enol and phenol (C–O) stretching vibrations [32]. The absorption band centered at 1161 cm^{-1} is correspond to the in-plane deformation vibration of phenyl rings. The peak at 1026 cm^{-1} is related to (C–O–C) vibration and benzoate trans-CH vibration at 961 cm^{-1}[31]. The peak at 864 cm^{-1} belongs to the C–H out-of-plane vibration of aromatic rings. The IR band at 820 cm^{-1} assigned to the highly mixed (CH) and aromatic (C–CH) bending vibrations [31]. The out-of-plane vibrations of OH groups are found at 458 cm^{-1} [31, 32].

3.3 X-ray diffraction (XRD)

The XRD patterns of CaO/SiO_2-L81, CaO/SiO_2-L61, CaO/SiO_2-L31 and curcumin-Ca(II)/SiO_2-L81 are shown in Fig. 2a-d, respectively. XRD patterns (Fig. 2a-c) exhibit strong reflection peaks corresponding to a face centered cubic crystal structure of CaO (*) [34], hexagonal crystals structure of $Ca(OH)_2$ ($) and $CaCO_3$ (♦) [35]. The obtained XRD patterns show that a reflection peaks at $2\theta = 32.7°$, 54.2°, 64.2°, and 68.7° corresponding to (111), (202), (311), and (222) lattice planes can be indexed as face-centered cubic structure of CaO (JCPDSPDF# 82-1690), respectively [34]. Some calcite peaks ($CaCO_3$ with low intensity are presented in the XRD pattern of CaO, illustrated rapid carbonation of

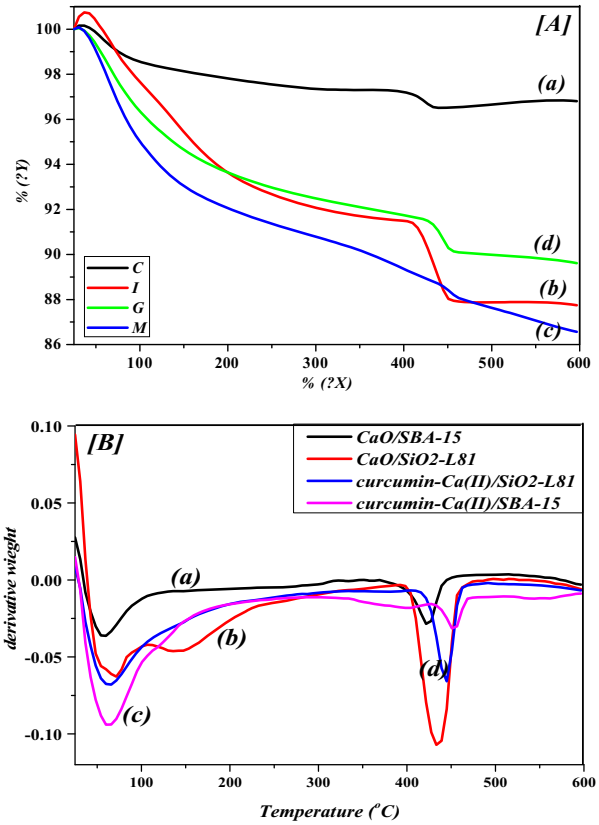

Fig. 6 **a** TGA and **b** DTA pattern of **a** CaO/SBA-15, **b** CaO/SiO_2-L81, **c** curcumin-Ca(II)/SBA-15, and **d** curcumin-Ca(II)/SiO_2-L81

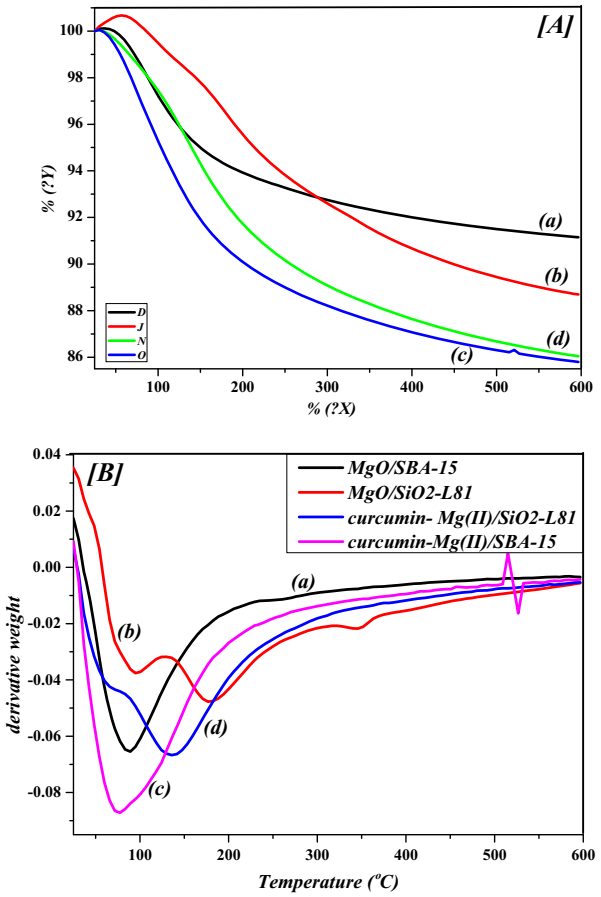

Fig. 7 **a** TGA and **b** DTA pattern of **a** MgO/SBA-15, **b** MgO/SiO_2-L81, **c** curcumin-Mg(II)/SBA-15, and **d** curcumin-Mg(II)/SiO_2-L81

CaO by atmospheric CO_2 [36]. All CaO diffraction peaks were observed for all types of materials with a little difference in intensity of the reflection peaks. After the interaction between CaO/SiO_2-L81 with curcumin, XRD pattern (Fig. 2d) exhibits reflection peaks corresponded to face-centered cubic structure of CaO (*) and hexagonal structure of Ca $(OH)_2$($) and almost $CaCO_3$ (♦) reflection peaks are disappeared [35]. The intensity of peaks corresponding to CaO decreases after interaction with curcumin. The obvious reason for this behavior is that only the surface CaO-NPs are in access for complexation with curcumin, but entrapped of CaO-NPs are not accessible for curcumin molecules. This is the reason behind that CaO-NPs at the surface are mostly converted to $CaCO_3$ which were consumed for the complexation with curcumin. Further evidence for the involvement of $CaCO_3$ in complexation with curcumin is confirmed by TGA (Fig. 6), where there was a reduction of CO_2 weight loss peak after treatment with curcumin.

The XRD patterns of MgO/SiO_2-L81, MgO/SiO_2-L61, MgO/SiO_2-L31 andcurcumin-Mg(II)/SiO_2-L81 are represented in Fig. 3a-d), respectively. In Fig. 3b, c), all diffraction peaks of XRD matched with a face-centered cubic structure (JCPDS card no.87-0653) [37, 38]. The major reflections at 2θ values of 36.74°, 42.8°, 62.3°, 74.6°, and 78.6° can be indexed to the lattice planes of (111), (200), (220), (311), and (222) planes reflections, respectively [37, 38]. The absence of any diffraction peaks related to Mg $(OH)_2$ and impurities in the XRD patterns may confirm high purity of the synthesized materials. No diffraction peaks were detected for MgO/SiO_2-L81 (Fig. 3a) in comparison with that of MgO/SiO_2-L61 and MgO/SiO_2-L31. The absence of the peaks for XRD pattern of MgO/SiO_2-L81 suggests that the MgO-NPs may present in non-crystalline form or that MgO-NPs present in small clusters in the pores of silica networks [39]. No diffraction peaks were detected for curcumin-Mg(II)/SiO_2-L81(Fig. 3d) and for MgO/SiO_2-L81 (Fig. 3a). The absence of these peaks does not give an obvious indication about the formation of curcumin-Mg(II) complex.

3.4 Small angle X-ray scattering (SAXS)

Figure 4a-c show SAXS patterns of SiO_2-L81 and its supported metal oxides CaO/SiO_2-L81 and MgO/SiO_2-L81, respectively.SiO_2-L81 (Fig. 4a) material exhibits a typical pattern of Lamellar structure with the occurrence of two

Table 1 Weight loss step and temperature of CaO and MgO oxides supported mesoporous silica and their curcumin complexes

Compound	Adsorbed water		Crystallized water		Dehydroxylation of $Ca(OH)_2$		Silica condensation and curcumin decomposition	
	T (°C)	Weight loss %	T (°C)	Weight loss %	T (°C)	Weight loss %	T (°C)	Weight loss %
CaO/SBA-15	75	2.3	–	–	430	0.7	>200	0.4 and –
CaO/SiO_2-L81	75	3	150	4	430	3.5	>200	2.0 and –
Curcumin-Ca(II)/SBA-15	65	6.5	–	–	430	0.5	>200	6.5
Curcumin-Ca(II)/SiO_2-L81	65	4.5	–	–	430	1.5	>200	4.5

Compound	Adsorbed water		Crystallized water		Silica condensation		Curcumin decomposition	
	T (°C)	Weight loss %	T (°C)	Weight loss %	T (°C)	Weight loss %	T (°C)	Weight loss %
MgO/SBA-15	80	6.5		–	>200	2.5	–	–
MgO/SiO_2-L81	95	1.5	176	4.5	>200	5	–	–
Curcumin-Mg(II)/SBA-15	75 (°C)	9 %	>200	0.5	>200	4.8		
Curcumin-Mg(II)/SiO_2-L81	75	2.5	135	6.5	>200	0.8	>200	4.0

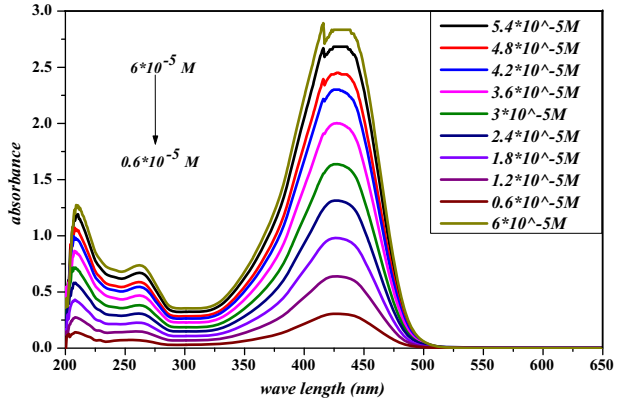

Fig. 8 UV–vis spectra of different curcumin concentration for standard curve

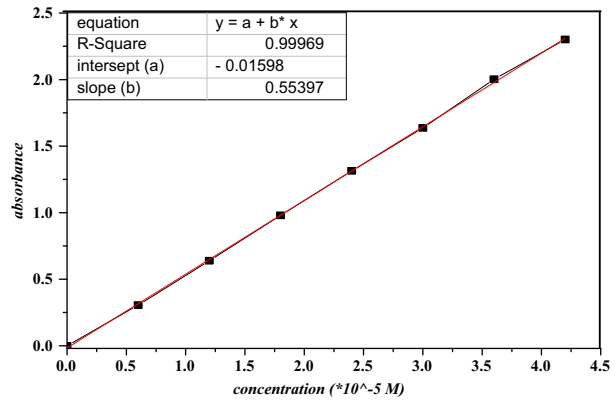

Fig. 9 Curcumin standard curve

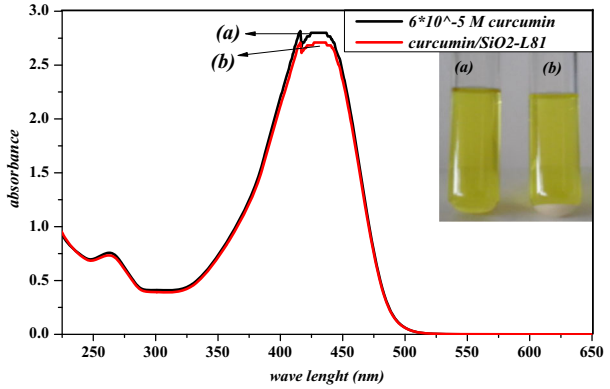

Fig. 10 UV-vis spectra of **a** curcumin and **b** curcumin/SiO_2-L81 after 72 h(s)

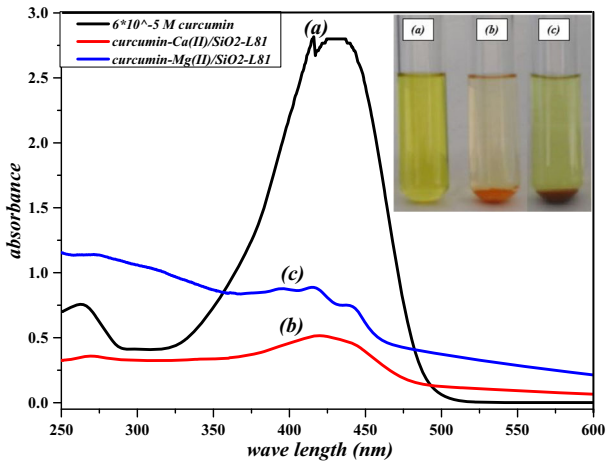

Fig. 11 UV–vis spectra of **a** curcumin, **b** curcumin-Ca(II)/SiO_2-L81, and **c** curcumin-Mg(II)/SiO_2-L81 after 72 h(s)

broad reflection peaks correspond to (001) and (002) planes [24]. SAXS patterns of CaO/SiO_2-L81 and MgO/SiO_2-L81 (Fig. 4b, c) showed a decreasing in the intensity of all reflections. The absence of the reflection peak due to (001) plane in the pattern of CaO/SiO_2-L81 and MgO/SiO_2-L81 (Fig. 4b, c) upon impregnated MO-NPs into SiO_2-L81 may

Table 2 Curcumin uptake capacity of curcumin

Sample	mg(cur)/0.2 g sample	Sample	Cur(mg)/0.2 g sample
SBA-15/CaO	20.2	SBA-15/MgO	18.9
L81/CaO	19.4	L81/MgO	17.8
L61/CaO	18.3	L61/MgO	16.4
L31/CaO	17.2	L31/O	15.5

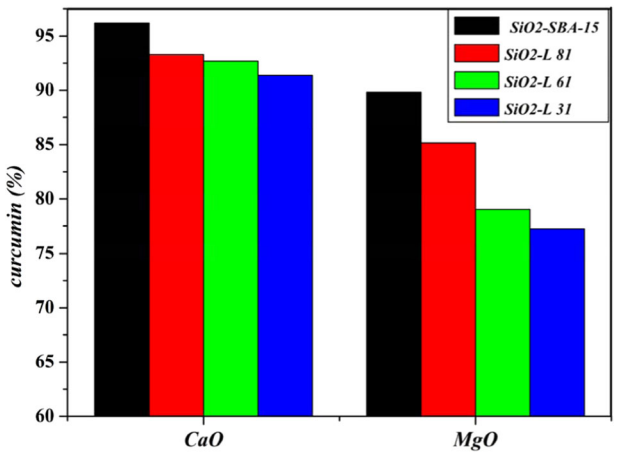

Fig. 12 Curcumin uptake (%) by CaO/mesoporous silica and MgO/mesoporous silica after 72 h(s)

distorted the lamellar structure of SiO_2-L81 (Fig. 4a) [39, 40]. The decrease of the peaks intensity of (002) reflection plane is expected due to the encapsulation of CaO and MgO into the pores, which may lead to reduce the scatter contrast between pore walls and pore space for the Bragg reflections [39, 41]. SAXS analysis of supported CaO and MgO/SBA-15 are well established [39, 40]. One major reflection peak observed for all support materials corresponded to the (100) diffraction peak, with two minor peaks assigned to (110) and (200) planes. It reflected the ordered structure of 2D hexagonal space group (p6mm) after impregnation of metal oxide [39].

3.5 Transmission electron microscopy (TEM)

TEM image of SiO_2-L81, CaO/SiO_2-L81, and MgO/SiO_2-L81 materials are given in Fig. 5a-d. TEM image of SiO_2-L81 (Fig. 5a) shows a wormhole-like mesoporous silica structure. The high-resolution image of SiO_2-L81 (Fig. 5b) shows an overlapping of layers confirming the presence of lamellar structure of SiO_2-L81, which is in a good agreement with SAXS results [26]. High-resolution TEM image of CaO/SiO_2-L81 (Fig. 5c) shows the channel of mesoporous silica in gray, while dark color CaO-NPs are probably absorbed into the mesopores of silica. Fig. 5d shows TEM image of MgO/SiO_2-L81, the MgO nanoclusters are seen in black, where some of MgO are absorbed into channels and other of MgO are appeared on the surface of mesoporous silica. TEM images of supported CaO and MgO/SBA-15 are well established [24, 39], so we are limited to report TEM images of supported CaO and MgO/lamellar mesoporous silica.

3.6 Thermal gravimetric analysis (TGA)

TGA and differential thermogravimetric analysis (DTA) for encapsulated CaO and MgO/mesoporous silica and their curcumin complexes are examined under nitrogen at 25–600 °C at rate 10 °C/min (Figs. 6 and 7). The thermogram of CaO/SBA-15, CaO/SiO_2-L81, curcumin-Ca(II)/SBA-15 and curcumin-Ca(II)/SiO_2-L81 (Fig. 6a-d) shows two main weight loss steps. The first step occurs at 75–150 °C due to loss of absorbed and crystallized water from the silica pores and CaO surface, respectively. The second step occurs at >200 °C. This is attributed to dehyroxylation of $Ca(OH)_2$ at 430, silica condensation and curcumin decomposition [35, 40–42]. The detailed specifications are summarized in Table 1.

The thermogram of MgO/SBA-15, MgO/SiO_2-L81 and their curcumin-Mg(II)/SBA-15 curcumin-Mg(II)/SiO_2-L81 are depicted in Fig. 7a-d). Two main weight loss steps are observed. The first step occurs at 75–200 °C due to loss of absorbed and crystallized water from the silica pores and MgO surface, respectively. The second step occurs at >200 °C. This is attributed to silica condensation and curcumin decomposition [41–46]. The detailed specifications are summarized in Table 1.

3.7 Ultraviolet-visible spectroscopy (UV–vis)

Figure 8 shows UV–vis spectra of curcumin with different concentrations. A UV–vis spectrum of the curcumin in ethanol shows absorption maximum at 429 nm assigned to the band $\pi \rightarrow \pi^*$. As concentration decrease, the absorbance also decrease. The spectrum is maintained the absorption peak at 429 nm.

Figure 9 shows the standard curve of curcumin. The relation between absorbance

and concentration is linear.

Figure 10a, b shows UV–vis spectra of curcumin and curcumin/SiO_2-L81. The UV–vis spectra of curcumin/SiO_2-L81 (Fig. 10b) shows an absorption maximum at 429 nmassigned to the band $\pi \rightarrow \pi^*$ [45]. It is clear that SiO_2-L81 uptake of curcumin from its ethanolic solution is almost zero due to its high hydrophbicity character.

Figure 11a-c shows UV–vis spectra of curcumin, curcumin-Ca(II)/SiO_2-L81 andcurcumin-Mg(II)/SiO_2-L81, respectively.

UV–vis spectrum of curcumin in ethanol shows absorption maximum at 429 nm assigned to the band $\pi \rightarrow \pi^*$ [44]. For the curcumin-M(II) complex (Fig. 11b, c), the maximum absorption peak of curcumin decreases due to the formation of curcumin—metal (II) complexes [46].

Table 2 and Fig. 12 showed curcumin uptake capacity for CaO/SiO_2 or MgO/SiO_2 with different mesoporous silica systems (SBA-15, SiO_2-L81, SiO_2-L61, and SiO_2-L31). It describes the curcumin uptake capacity as cur(mg)/0.2 g sample for all metal oxide/mesoporous silica systems. There is a decreasing of curcumin uptake in the following order:

$$SBA-15 > SiO_2-L81 > SiO_2-L61 > SiO_2-L31$$

4 Conclusion

Supported metal oxides (CaO and MgO) into mesoporous silica were synthesized via impregnation method. Curcumin uptake (%) with supported metal oxides/mesoporous silica was determined by batch method. These materials were investigated by several characterization techniques FTIR, XRD, SAXS, TEM, TGA, and UV–vis. FTIR spectra of supported metal oxide mesoporous silica confirmed that metal oxides were physically bonded with silanol groups. TEM images showed that metal oxides are loaded inside the silica mesopores. SAXS analysis showed that metal oxides (CaO and MgO) are introduced onto/into the mesoporous silica and altered the mesoscopic structure. XRD showed that all metal oxides were in crystalline form faced center cubic CaO and MgO, except that encapsulated inside the mesopores of SiO_2-L81. XRD analysis shows that not all metal oxides react with curcumin. This is confirmed by a slight decrease of all diffraction peaks intensity of metal oxides. UV–vis analysis and curcumin uptake studies confirm that the curcumin uptake capacity is depended on the nature of metal oxides and the nature of mesoporous silica. It is found that CaO/SBA-15 was the best for curcumin uptake of 96.5%.

Acknowledgements The authors would like to express their sincere thanks for the Chemistry Department, Al Azhar University of Gaza for its financial support.

Compliance with ethical standards

Conflict of interest The authors declare that they have no conflict of interest.

References

1. Ruby A, Kuttan G, Babu K, Rajasekharan K, Kuttan K (1995) Anti-tumour and antioxidant activity of natural curcuminoids. Cancer Lett 94:79
2. Lantza R, Chena G, Solyomb A, Jolad S, Timmermann B (2005) The effect of turmeric extracts on inflammatory mediator production. Phytomedicine 12:445.
3. Patra D, Barakat C (2011) Synchronous fluorescence spectroscopic study of solvatochromic curcumin dye. Spectrochim Acta Part A Mol Biomol Spectrosc 79:1034
4. Yang F, Lim G, Begum A, Ubeda O, Simmons M, Ambegaoka S, Chen P, Kayed R, Glabe C, Frautschy S, Cole G (2005) Curcumin inhibits formation of amyloid β oligomers and fibrils,binds plaques, and reduces amyloid in vivo. J Biol Chem 280:5892
5. Egan M, Pearson M, Weiner S, Rajendran V, Rubin V, Glöckner-Pagel J, Caplan M (2004) Curcumin, a major constituent of turmeric, corrects cystic fibrosis defects. Science 304:600
6. Maheshwari R, Sing A, Gaddipati J, Srimal R (2006) Multiple biological activities of curcumin: a short review. Life Sci 78:2081
7. Krishnaswamy K, Raghuramulu N (1998) bioactive phytochemicals with emphasis on dietary practices. Indian J Med Res 108:167
8. Pang S, Tay S, Chin S (2014) Facile synthesis of curcumin-loaded starch-maleate nanoparticles. J Nanomater 2014:22
9. Basniwal R, Hr B, Jain V, Jain N (2011) Curcumin nanoparticles: preparation, characterization, and antimicrobial study. J Agric Food Chem 59:2056
10. Kotcherlakota R, Barui AK, Prashar S, Fajardo M, Briones D, Rodríguez-Diéguez A, Patra CR, Gómez-Ruiz S (2016) Curcumin loaded mesoporous silica: an effective drug delivery system for cancer treatment. Biomater Sci 4(2016):448
11. Das SK, Bhunia MK, Chakraborty D, Khuda-Bukhsh AR, Bhaumik A (2012) Hollow spherical mesoporous phosphosilicate nanoparticles as a delivery vehicle for an antibiotic drug. Chem Commun 48(2012):2891–2893
12. Modasiya M, Patel V (2012) Studies on solubility of curcumin. Int J Pharm Life Sci 3:1490
13. Wang A, Muhammad F, Qi W, Wang N, Chen L, Zhu G (2014) Acid-induced release of curcumin from calcium containing nanotheranostic excipient. ACS Appl Mater Interfaces 6:14377
14. Muhammad F, Wang A, Guo M, Zhao J, Qi W, Yingjie G, Gu J, Zhu G (2013) pH dictates the release of hydrophobic drug cocktail from mesoporous nanoarchitecture. ACS Appl Mater Interfaces 5:11828
15. C. Kresge C, Leonowicz M, Roth W, Vartuli J, Beck J (1992) Ordered mesoporous molecular sieves synthesized by a liquid crystal template mechanism. Nature 359:710
16. Slowing I, Vivero-Escoto J, Wu C, Lin V (2008) Mesoporous silica nanoparticles as controlled release drug delivery and gene-transfection carriers. Adv Drug Deliv Rev 60:1278
17. Lam K, Yeung K, McKay G (2005) Mesoporous silica nanoparticles as controlled release drug delivery and genetransfection carriers. NSTI-Nanotech 2:273
18. Barreca D, Blau W, Croke G, Deeney F, Dillon F, Holmes J, Tondello J (2007) Iron oxide nanoparticle impregnated mesoporous silicas asplatforms for the growth of carbon nanotubes. Microporous Mesoporous Mater 103:142
19. Hornebecq V, Antonietti M, Cardinal T, Treguer-Delapierre M (2003) Stable silver nanoparticles immobilized in mesoporous silica. Chem Mater 15:1993
20. Li Z, Barnes J, Bosoy A, Stoddart J, Zink J (2012) Mesoporous silica nanoparticles in biomedical applications. Chem Soc Rev 41:2590

21. Roggenbuck J, Waitz T, Tiemann M (2008) Synthesis of mesoporous metal oxides by structurereplication: strategies of impregnating porous matrices with metal salts. Microporous Mesoporous Mater 113:575
22. Furtado A, Wang Y, Glover T, LeVan D (2011) MCM-41 impregnated with active metal sites: Synthesis, characterization, and ammonia adsorption. Microporous Mesoporous Mater 142:730
23. Lee J, Chang J (2012) Highly ordered magnetic mesoporous silicas for effective elimination of carbonmonoxide. J Solid State Chem 188:100
24. Wang Y, Wu Y, Wei Y, Zhu J (2005) In situ coating metal oxide on SBA-15 in one-pot synthesis. Microporous Mesoporous Mater 84:127
25. Lee H, Kim W, Lee J, Choi D, Jeong Y, Chang J (2012) Transition metal-chelating surfactant micelle templates for facile synthesis of mesoporous silica nanoparticles. J Solid State Chem 185:89
26. El-Nahhal I, Salem I, Tabasi Hempelmann N, Kode F (2018) Synthesis and structural characterization of ZnO-and CuO-NPssupported mesoporous silica materials (hexagonal SBA-15and lamellar-SiO2). Chem Phys Lett 691:165
27. Sundar S, Mariappan R, Piraman S (2014) Synthesis and characterization of amine modified magnetite nanoparticles as carriers of curcumin-anticancer drug. Powder Technol 266:321
28. Wanyika H, Gatebe E, Kioni P, Tang Z, Gao Y (2011) Synthesis and characterization of ordered mesoporous silica nanoparticles with tunable physical properties by varying molar composition of reagents. Afr J Pharm Pharmacol 5:2402
29. Li Y, Sun N, Li L, Zhao N, Xiao F, Wei W, Sun Y, Huang W (2013) Grafting of Amines on Ethanol-Extracted SBA-15 for CO2 Adsorption. Materials 6:981
30. Das S (2011) Immobilization of enzymes in sol-gel mesoporous silica, enzymatic digestion of biomass, and silica-curcumin hybrid materials. Doctoral dissertation, Drexel University, p 125.
31. Subhan M, Alam K, Rahaman M, Rahman M, Awal R (2013) Synthesis and characterization of metal complexes containing curcumin (C21H20O6) and study of their anti-microbial activities and DNA binding properties. J Sci Res 6:97
32. Mohan P, Sreelakshmi G, Muraleedharan C, Joseph R (2012) Water soluble complexes of curcumin with cyclodextrins: characterization byFT-Raman spectroscopy. Vib Spectrosc 62:77
33. Gangwar R, Tomar G, Dhumale V, Zinjarde S, Sharma R, Datar S (2013) Curcumin conjugated silica nanoparticles for improving bioavailability and its anticancer applications. J Agric Food Chem 61:9632
34. Imtiaz A, Farrukh MA, Khaleeq-ur-Rahman M, Adnan R (2013) Micelle-assisted synthesis of Al2O3·CaO nano catalyst: optical properties and their applications in photo degradation of 2,4,6-trinitrophenol. Sci World J. https://doi.org/10.1155/2013/641420.
35. Stutzman PE (1996) Guide for X-ray powder diffraction analysis ofPortland cement and clinker, National Institute of Standards and Technology, (NISTIR) Gaithersburg, 5755.
36. Mirghias Z, Bakhtiari F, Darezereshki E, Esmaeilzadeh E (2014) Preparation and characterization of CaO nanoparticles from Ca (OH)2by direct thermal decomposition method. J Ind Eng Chem 20:113
37. Salem J, El-Nahhal I, Hammad T, Kuhn S, Sharekh S, M. Askalani M, Hempelmann M (2015) Optical and fluorescence properties of MgO nanoparticles in micellarsolution of hydroxyethyl laurdimonium chloride. Chem Phys Lett 636:26
38. Hadia N, Mohamed H (2015) Characteristics and optical properties of MgO nanowires synthesized by solvothermal method. Mater Sci Semicond Process 29:238
39. Wang N, Yu X, Shen K, Chu W, Qian W (2013) Synthesis, characterization and catalyticperformance of MgO-coated Ni/SBA-15 catalysts for methane dry reforming to syngas and hydrogen. Int J Hydrog Energy 38:9718
40. Huang C, Chang K, Yu C, Chiang P, Wang C (2010) Development of high-temperature CO2 sorbents made of CaO-based mesoporous silica. Chem Eng J 161:129
41. Sun H, Han J, Ding Y, Li W, Daun J, Chen P, Lou H, Zheng X (2010) One-pot synthesized mesoporous Ca/SBA-15 solid base for transesterification of sunflower oil with methanol. Appl Catal A 390:26
42. Butt A, Ejaz S, Baron J, Ikram M, Alia S (2015) CaO Nanoparticles as a potential drug delivery agent for biomedical applications. Dig J Nanomater Biostructures 10:799
43. Zhang D, Ordered J (2013) SBA-15 mesoporous silica with highamino-functionalization for adsorption of heavy metal ions. Chin Sci Bull 58:879
44. Maoz B, Tirosh E, Sadan M, Markovich G (2011) Defect-induced magnetism in chemically synthesized nanoscale sheets of MgO. Phys Rev B 83:161201
45. Azzaza S, El-Hilo M, Narayanan S, Vijaya Mamouni J, Benyoussef A, Bououdina A (2014) Structural, optical and magnetic characterizations of Mn-doped MgO nanoparticles. Mater Chem Phys 143:1500
46. Zebib B, Mouloungui Z, Noirot V (2010) Stabilization of curcumin by complexation with divalent cations in glycerol/water system. Bioinorg Chem Appl. https://doi.org/10.1155/2010/292760.